New insights into the mesophase transformation of ethane-bridged PMOs by the influence of different counterions under basic conditions

Reference:

Lin Feng, Meng, Kukueva Elena, Mertens Myrjam, Van Doorslaer Sabine, Bals Sara, Cool Pegie.- New insights into the mesophase transformation of ethane-bridged PMOs by the influence of different counterions under basic conditions
RSC advances - ISSN 2046-2069 - 5:8(2015), p. 5553-5562
DOI: http://dx.doi.org/doi:10.1039/c4ra15849k

Journal Name

RSCPublishing

ARTICLE

Cite this: DOI: 10.1039/xoxxoooooox

New insights into the mesophase transformation of ethane-bridged PMOs by the influence of different counterions under basic conditions

Received ooth January 2012,
Accepted ooth January 2012

DOI: 10.1039/xoxxoooooox

www.rsc.org/

Feng Lin,[a,b] Xiangyan Meng,[a] Elena Kukueva,[c] Myrjam Mertens,[d] Sabine Van Doorslaer,[b] Sara Bals,[c] and Pegie Cool[a*]

The counterions are of crucial importance in determining the mesostructure and morphology of ethane-bridged PMO materials synthesized under basic conditions. By using CTABr as the surfactant, the final PMO materials show a 2-D hexagonal (*p6mm*) mesophase, while PMO materials with cubic ($Pm\overline{3}n$) mesostructure are obtained when CTACl or $CTA(SO_4)_{½}$ are used. With gradually replacing CTABr by CTACl or $CTA(SO_4)_{½}$ while keeping the total surfactant concentration constant, a clear *p6mm* to $Pm\overline{3}n$ mesophase evolution process is observed. For a given gel composition, the mesophase of ethane-bridged PMO materials can also be adjusted by the addition of different sodium salts. To be brief, the effect of the counterions on the mesophase can be attributed to the binding strength of the ions on the surfactant micelles, which follows the Hofmeister series (SO_4^{2-} < Cl^- < Br^- < NO_3^- < SCN^-). Furthermore, it is found that the hydrolysis and condensation rate of the organosilica precursor also plays an important role in the formation of the final mesostructure

Introduction

Using the surfactant-templating-based synthesis approach, a large number of mesoporous silica materials with uniform pore size and very high surface areas have been synthesized, which have great potential for catalysis,[1-4] adsorption,[5,6] drug delivery,[7,8] sensing,[7,9] etc. Since the composition, the microscopic structure and macroscopic morphology of a material are of crucial importance in determining its properties and functions, novel practical applications require the structural and morphological control of these mesoporous silica materials. In general, mesoporous silica materials are synthesized through the hydrolysis and condensation of a silica precursor under basic or acidic conditions, in the presence of a structure-directing agent. The formation of the ordered mesostructure involves a comparatively complex chemical process, including the hydrolysis and condensation of silicate, self-assembly of the surfactant, electrostatic interactions, and so on. Among these, the packing of the surfactants and the charge density matching between the silica species and surfactant micelles always play a major role in determining the mesostructure of the final materials.[10] It has been reported that, during the self-assembly process, the mesostructure can be controlled by varying the surfactant (type and concentration), counterions and pH of the reaction mixture, and adding co-solvent/co-surfactant, etc.

Most of the previous studies on the effect of counterions on the formation of mesostructures were carried out under acidic conditions in the presence of cationic surfactants or block copolymers,[10-13] due to the fact of the weak surfactant/silicate interation. In the acidic synthesis route, the positively charged silicate species (I^+) are proposed to react with the surfactants (S^+or N^0) via the counteranions (X^-) through a $S^+X^-I^+$ or $(N^0H^+)X^-I^+$ type interaction, in which the counteranions play an important role to buffer the repulsion between $S^+/(N^0H^+)$ and I^+.[10] The variation of the counteranions at the interfacial region of the silica-surfactant has a significant effect on the formation of the final material. Lin et al.[14] have found that the morphology of the final material strongly depends on the use of different acid sources. Furthermore, they have noticed that the induction time for the formation of mesostructural precipitation increases in the lyotropic series HNO_3< HBr< HCl< H_2SO_4 under the same acid concentration, whereas the structural ordering of the as-synthesized hexagonal phase follows a sequence of HNO_3> HBr> HCl> H_2SO_4.[14] Actually, the variation of the counterion can not only affect the induction time and the structural ordering of the final material, but also leads to the formation of different mesophases. By using cetyltriethylammonium bromide

(CTEABr) as the cationic template, Che et al.[11] have prepared four types of mesophases including 3-D hexagonal $P6_3/mmc$, cubic $Pm\bar{3}n$, 2-D hexagonal *p6mm* and cubic *Ia3d*, in the presence of H_2SO_4, HCl, HBr and HNO_3, respectively. Zhao et al.[13] have reported a 2-D hexagonal *p6mm* to cubic *Ia3d* mesophase evolution by simply adjusting the acidity and/or counterions in the presence of block copolymers (P123). Moreover, it is found that the counterions sequence that induces structural change is quite different between the non-ionic block copolymer and ionic surfactant templating systems. Recently, through a detailed study of the structural changes of the as-made mesostructured silica prepared using cetyltriethylammonium bromide (CTEABr) as surfactant in acidic conditions, Liu et al.[15] have found that the counterions present in the interfacial space between the pore-directing CTEA micelle and the silica wall are ready to be exchanged, accompanied by phase transformation and morphology change.

Under basic conditions, the mesostructure is constructed by the negatively charged silicate species (I^-) and the surfactants (S^+) through the strong S^+I^- electrostatic interaction, in which the counterions X^- are not directly involved. Thus, in this case, the role of the counterions on the formation of mesostructure is less pronounced compared with the one obtained via the acidic synthesis route, and less attention is thus paid to the study of the effect of counterions. Through the addition of different sodium salts, Lin et al.[16] found that, at the same concentration, the induction time for the formation of a mesophase increases in the sequence of $Cl^-<SO_4^{2-}<Br^-<NO_3^-$, which is almost reverse to that of the sequence under acidic conditions. They have also pointed out that the morphology of the final material is different according to different counterions.[17] With the assistance of different counterions, Bonneviot el al.[18] have found that the structure of mesoporous silica can be tuned from lamellar *P2* to 2-D hexagonal *p6mm*, depending on the pH value of the synthetic system. However, up to now, no mesophase changes were observed upon variation of the counterions during the synthesis of mesoporous silica under basic conditions.

Periodic mesoporous organosilica (PMO) materials,[19-21] characterized by their ordered mesoporous structures and inorganic-organic hybrid frameworks, are considered a very interesting breakthrough in the field of mesoporous materials. Due to the combination of organic and inorganic components, PMOs have some unique properties compared with the pure-silica mesoporous material, such as the tunable surface hydrophobicity, and enhanced mechanical and hydrothermal stability.[22] However, in contrast to the pure-silica mesoporous materials, the studies on the structure and morphology control of PMO materials are still scarce, regardless of the potential of PMO materials. Generally speaking, the approaches for the control of mesostructure of pure-silica mesoporous materials can be also applied for PMO materials, such as using different surfactants[23-25], varying the pH of the mixture[26,27] and adding co-solvent/co-surfactant[28-30]. But due to the hydrophobic moieties in the organosilica precursor, the interfacial energies between template and precursor as well as the charge density is distinctly different from pure-silica precursors. In addition, considering the steric, conformation and bond angle constraints imposed by the organic groups, the self-assembly process is actually much more challenging for organosilicas.

In the present study, we report a facile mesophase control of ethane-bridged PMOs under basic conditions. It is found that, under S^+I^- synthesis pathway, counterions are of crucial importance in determining the structure and morphology of PMO materials. A *p6mm* to $Pm\bar{3}n$ mesophase evolution can be achieved simply by varying the counterions of the synthetic system. To the best of our knowledge, this is the first report on the mesophase transformation simply induced by counteranions under basic conditions, in the presence of cationic surfactant. Our findings lead to a further understanding of the formation mechanism of PMO materials. Furthermore, we found that the hydrolysis and condensation rate of the organosilica precursor also plays a role in influencing the mesostructure of the final product.

Experimental

Materials

All starting materials were used as purchased without further purification: 1,2-bis(trimethoxysilyl)-ethane (BTME, 96% Sigma-Aldrich), 1,2-bis(triethoxysilyl)-ethane (BTEE, 96% Sigma-Aldrich), cetyltrimethylammonium chloride (CTACl, 98% Sigma-Aldrich), cetyltrimethylammonium bromide (CTABr, 99% Sigma-Aldrich), cetyltrimethylammonium chloride ($CTA(SO_4)_{½}$, 98% Xiamen Pioneer Technology Co., LTD.), NaOH (98.5% Acros Organic), NaCl (99.8% Sigma-Aldrich), $NaNO_3$ (99% Acros Organic), NaSCN (98% Sigma-Aldrich)

Synthesis of PMO materials

Ethane-bridged PMO materials were synthesized according to the article of Inagaki et al.[19] and Sayari et al.[31] with some minor adjustments, using the synthesis mixtures with the following composition: 1.0 BTEE : 0.57 CTAx : 2.36 NaOH : 353 H_2O, where x refers to Br^-, Cl^- or ½ SO_4^{2-}. In a typical synthesis, BTEE (2 ml) was added to a mixture of CTABr surfactant (1.09 g), sodium hydroxide (0.497 g), and distilled water (33.3 g) under vigorous stirring at ambient temperature. The mixture was stirred for another 24 h, and then heated at 95 °C for 20-24 h under static conditions, followed by filtration, and dried at room temperature. Surfactant template removal was accomplished by two solvent extraction cycles with acidic ethanol at 60°C. After filtration, the sample was washed thoroughly with ethanol and dried at room temperature.

In a series of experiments, CTABr was gradually replaced with CTACl or $CTA(SO_4)_{½}$ under the same experimental conditions while keeping the total surfactant concentration constant. In another series of experiments, different inorganic salts, including $NaNO_3$, NaCl and NaSCN, were added to the synthesis mixture, respectively, before the addition of the organosilica precursor. The amount of inorganic salts was controlled to be equimolar with the surfactant in the mixture. In the last part, BTME was used as the silica source instead of BTEE during the synthesis of the PMOs.

Methods

N_2 adsorption–desorption isotherms were obtained at liquid N_2 temperature (77 K) using a Quantachrome Quadrasorb-SI automated gas adsorption system. Prior to adsorption, the samples were outgassed under high vacuum for 16 hours at 100 °C. The specific surface area was calculated using the Brunauer-Emmet-Teller (BET) method, between a relative pressure of 0.05 and 0.35. The pore size distributions were deduced from the desorption branches of the isotherms using the Barrett-Joyner-Halenda (BJH) method. The total pore volumes were calculated from the amount of N_2 vapor adsorbed at a relative pressure of 0.95.

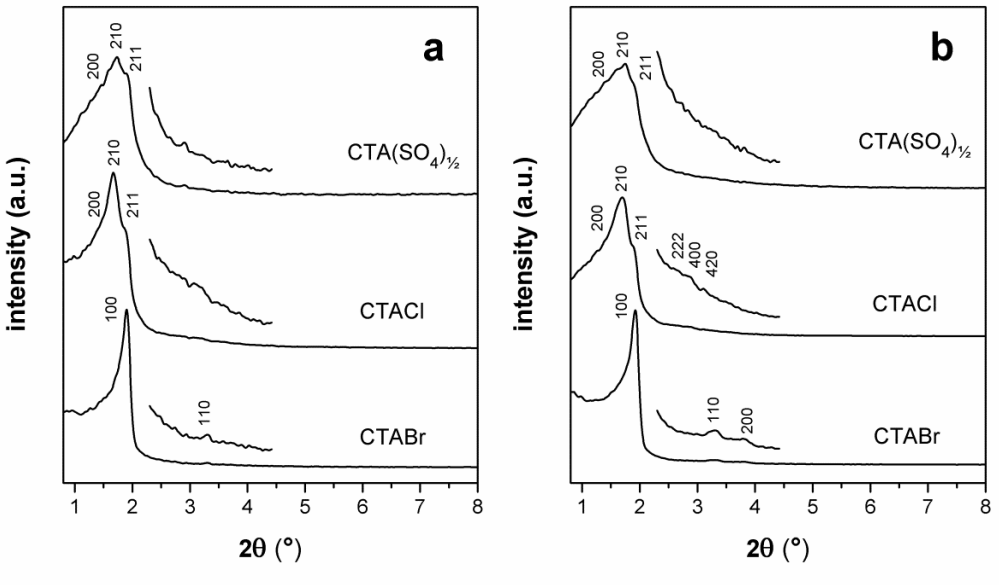

Figure 1. XRD patterns of ethane-bridged PMOs synthesized with different surfactants (a): as-synthesized and (b): solvent-extracted. All PMOs are prepared with the BTEE silica precursor.

X-ray diffraction (XRD) measurements were recorded on a Pananalytical X'PERT PRO MPD diffractometer with filtered CuKα-radiation. The measurements were performed in the 2θ mode using a bracket sample holder with a scanning speed of 0.04°/4 s continuous mode.

Scanning electron microscopy (SEM) images were acquired using FEI Quanta 250 operated at 3-5 kV and JSEM 5510 operated at 15 kV. For the transmission electron microscopy (TEM) measurements, the samples were dispersed in ethanol, crushed in an agate mortar and deposited on a carbon coated copper grid. TEM images and selected area electron diffraction (SAED) patterns were acquired using and FEI Tecnai instrument operated at 200 kV with camera length 3,5-4 m.

RESULTS

Effect of cetyltrimethylammonium surfactant with different counterions

Figure 1 shows the XRD patterns of as-synthesized and solvent-extracted ethane-bridged PMOs prepared with BTEE, in the presence of cetyltrimethylammonium surfactant with different counterions. Before solvent-extraction, the XRD pattern of the sample synthesized with CTABr shows two diffraction peaks in the low-angle region. Whereas the solvent-extracted sample exhibits three diffraction peaks, which could be assigned to (100), (110) and (200) diffractions of a typical 2-D hexagonal (*p6mm*) structure with a high degree of structural ordering. The ethane-bridged PMOs synthesized with CTACl shows an XRD pattern consistent with a cubic ($Pm\overline{3}n$) mesostructure, characterized by the (200), (210) and (211) diffractions. After solvent-extraction, the higher order peaks become more clear. For the sample prepared with CTA(SO4)½, the XRD pattern exhibits three diffraction peaks similar to that of the sample prepared with CTACl, indicating a cubic ($Pm\overline{3}n$) mesostructure. However, broader lines are observed for this sample, which is probably due to the poor structure ordering or the occurrence of some other mesophase.

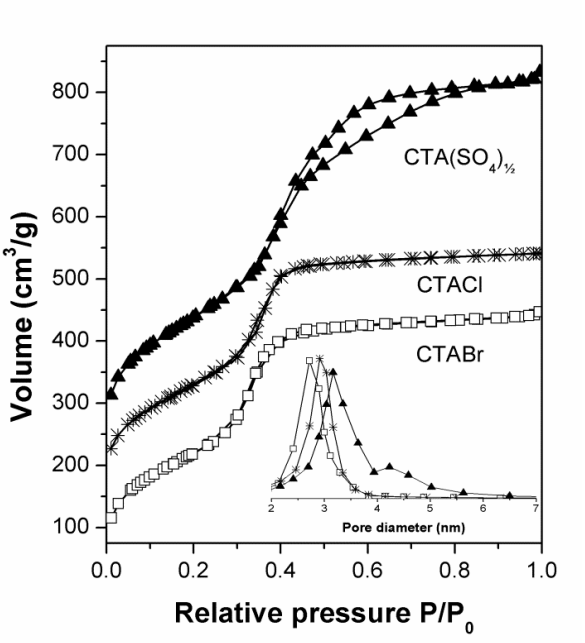

Figure 2. N_2 adsorption-desorption isotherms of the ethane-bridged PMOs synthesized with different surfactants and the corresponding pore-size distributions

The nitrogen adsorption-desorption isotherms and the corresponding pore-size distribution curves of the three samples are presented in figure 2, and the textural properties are summarized in table 1. All the samples exhibit type-IV isotherms with a well-defined capillary condensation step in the relative pressure (P/P_0)

range of 0.2~0.6, typical of mesoporous materials. This indicates that all of the samples possess a good mesostructural ordering and a uniform pore size. For the sample synthesized with $CTA(SO_4)_{½}$, the shape of the hysteresis loop resembles more the H2 type, which is usually attributed to a ink-bottle-shaped mesopore configuration.[24]

Table 1. The textural properties of ethane-bridged PMOs synthesized with different surfactants

Sample	CTABr	CTACl	$CTA(SO_4)_{½}$
Surface area(m^2g^{-1})	812	703	891
Pore size(nm)	2.7	3.0	3.2
Total Pore Volume (cm^3g^{-1})	0.684	0.605	0.961

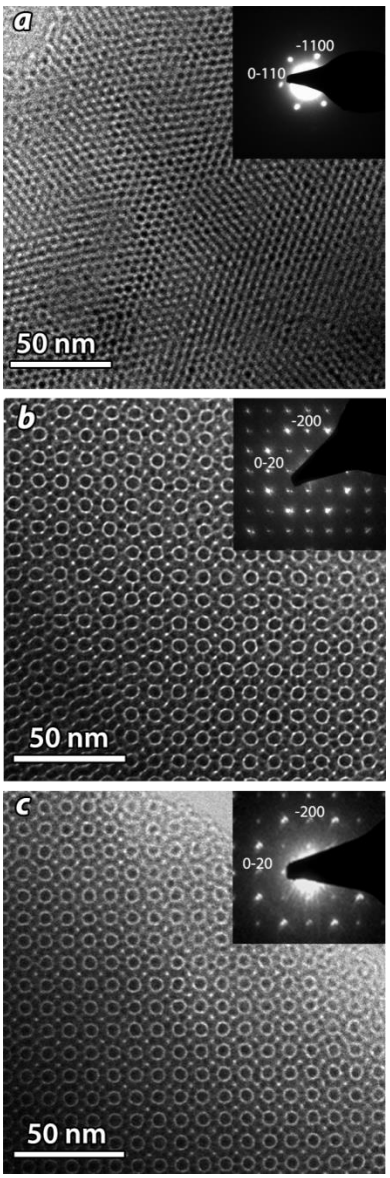

Figure 3. TEM images of the solvent-extracted PMOs synthesized with: (a) CTABr, (b) CTACl and (c) $CTA(SO_4)_{½}$, acquired along the [001] direction. The corresponding SAED patterns are presented as insets.

In order to confirm the mesostructures of these PMO materials, further evidence for their mesostructures is provided by the bright field TEM images and the corresponding electron diffraction (ED) patterns presented in figure 3. In case of CTABr surfactant, the images (figure 3a) illustrate the ordered arrays along the direction perpendicular to the pore axis, yielding similar symmetry in comparison to the mesostructures of MCM-41 and SBA-15. The ED pattern in figure 3a reveals a clear hexagonal pore arrangement, confirming the 2D hexagonal mesophase observed by XRD measurements. The TEM images of the samples prepared with CTACl and $CTA(SO_4)_{½}$ are shown in figure 3b and 3c, respectively. Both of the bright field TEM images exhibit square patterns, which confirms the cubic symmetry of the two samples. The ED patterns in the inset clearly show that the incident beam direction [100] supports a cubic ($Pm\overline{3}n$) mesostructure.

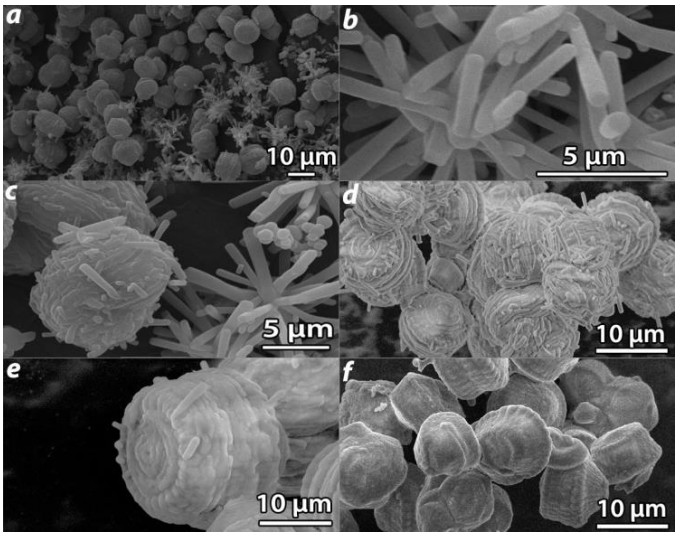

Figure 4. SEM images of ethane-bridged PMO sample synthesized with CTABr. (a) lower magnifications, (b-f) higher magnifications. All images are taken from the same batch.

The SEM images of the ethane-bridged PMO synthesized with CTABr are shown in figure 4, with all of the images in the figure being taken from the same sample batch. In the low magnification SEM image presented in figure 4a, particles with different morphology can be observed. One of the typical morphologies of this sample is presented in figure 4b, showing an urchin-like shape. Actually, this urchin-like morphology is less common for mesoporous silica materials. Cai et al.[32] reported an urchin-like MCM-41 which was synthesized in a NH_4OH medium. It is proposed that the urchin-like morphology was formed by the random deposition of the self-assembled silicate rod-like micelles.[32] Figure 4c shows the urchin-like particles and some irregular particle with many rods on the surface. The rods on the surface of these irregular particles are very similar to the rods observed in the urchin-like particles, which might indicate that the irregular particle is indeed formed by a highly twisted urchin-like particle. The particles shown in figure 4d and 4e are very similar to the irregular particle shown in figure 4c, except that the particles are more symmetric. Moreover, the surface of the particle shown in figure 4e is relatively smooth. Particles with symmetric gyroid morphology are shown in figure 4f, which is one kind of the typical morphologies of the 2D-hexagonal mesophase.[31,33,34] Since all SEM images in figure 4 are acquired from the same batch, however, it is reasonable to assume a

continuous evolution in the morphology with along a sequence that is illustrated in figure 4b, 4c, 4d, 4e and 4f.

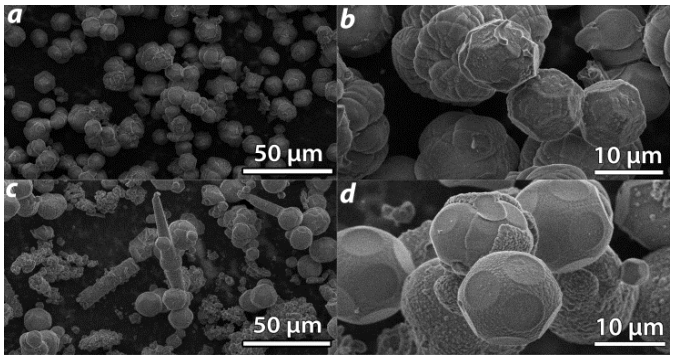

Figure 5. SEM images of ethane-bridged PMO samples synthesized with: (a, b) CTACl, (c, d) $CTA(SO_4)_{½}$

Generally speaking, the morphology of mesoporous silica materials is strongly dependent on their mesostructure. Figures 5a and 5b show the morphology of the PMOs synthesized with CTACl. This material consists only of agglomerated or isolated particles with well-defined external morphology of decaoctahedron, which is typical for mesoporous silica materials with a cubic ($Pm\bar{3}n$) mesostructure.[35,36] Although the PMO sample synthesized with $CTA(SO_4)_{½}$ also exhibits a cubic ($Pm\bar{3}n$) mesostructure, confirmed by XRD and TEM, it can be noticed that the morphology of this sample is different from the sample synthesized with CTACl, exhibiting a more spherical shape with some circular flat faces on the surface (figure 5c and 5d). In addition, some long-rod-like particles can be observed in this sample (Figure 5c).

The above results indicate that the mesophase and morphology of the final PMOs can be controlled by the change in counterions of the surfactant. In order to have a better understanding of the mesophase evolution upon variation of the counterions, a series of surfactant mixtures of CTACl/CTABr or $CTA(SO_4)_{½}$/CTABr was used to prepare ethane-bridged PMOs, keeping the total surfactant concentration constant.

Figure 6a shows the XRD patterns of the materials synthesized with BTEE in the presence of a surfactant mixture of CTACl/CTABr with different molar ratios. When the molar ratio CTACl : CTABr is 0:10 or 2:8, the XRD pattern of the sample exhibits an intense peak at around 2θ = 2.0°, which can be indexed to the (100) diffraction peak of 2-D hexagonal (*p6mm*) mesophase. For the sample synthesized with CTACl : CTABr = 4:6, the sharp (100) diffraction peak of the XRD pattern still indicates that this sample consists of mainly 2-D hexagonal (*p6mm*) mesophase. However, an additional tiny shoulder peak can be observed at 2θ = 1.6°. By further increasing the proportion of CTACl, the peak at 2θ = 1.6° grows stronger, and the XRD pattern of the sample synthesized with CTACl : CTABr = 6:4 clearly shows two diffraction peaks with similar intensity in the low angle region, which can neither be assigned to single 2-D hexagonal (*p6mm*) mesophase nor cubic ($Pm\bar{3}n$) mesophase, but a mixture of the two. This result is also confirmed by the SEM images (supporting information). When CTACl : CTABr = 8:2 or 10:0, the XRD pattern of the sample shows the existence of (210) and (211) diffractions, which are typical for a cubic ($Pm\bar{3}n$) mesostructure. These observations indicate that with gradually replacing CTABr by CTACl during the synthesis, the mesophase of the final PMOs was gradually transformed from a 2-D hexagonal (*p6mm*) mesostructure to a cubic ($Pm\bar{3}n$) mesostructure. It is also noteworthy that the (100) diffraction peak of the 2-D hexagonal structure changes continuously to the (211) diffraction peak of the cubic structure with changing molar ratio of the surfactant mixture. Figure 6b shows the XRD patterns of the PMO materials synthesized with the surfactant mixture of

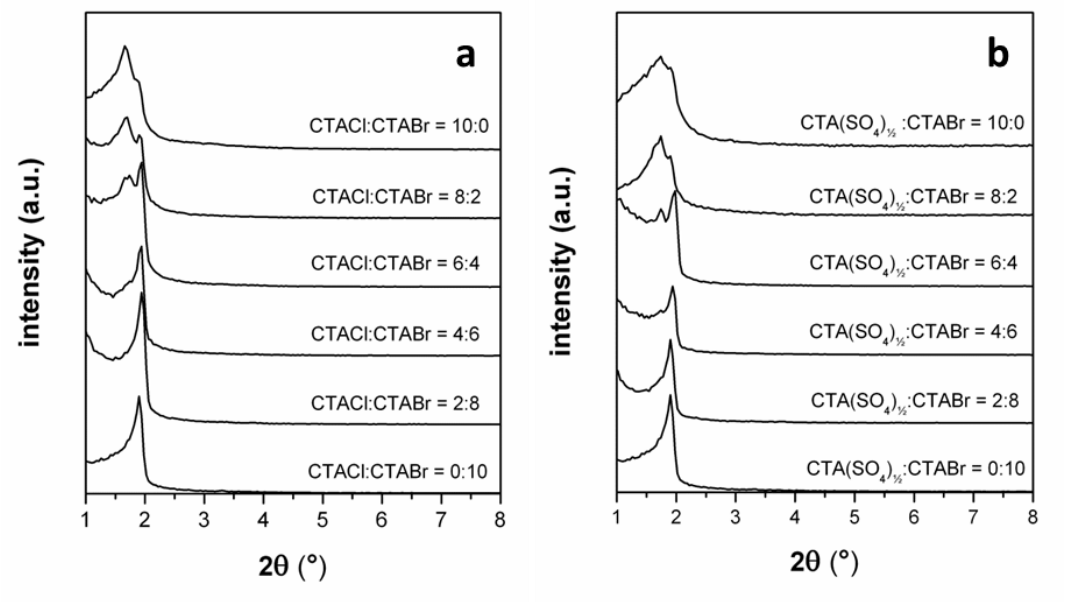

Figure 6. The evolution of the XRD patterns of as-synthesized ethane-bridged PMOs prepared with a surfactant mixture of (a) CTABr/CTACl and (b) $CTABr/CTA(SO_4)_{½}$ with different molar ratios. All PMOs are prepared with the BTEE silica precursor.

$CTA(SO_4)_{½}$/CTABr with different molar ratios. The evolution of the XRD pattern with the change of surfactant molar ratio is quite similar to that shown in figure 6a, indicating a gradual mesophase transformation from 2-D hexagonal (*p6mm*) structure to cubic ($Pm\bar{3}n$) structure.

Effect of different sodium salts

The above results show that by simply replacing the counterions of the surfactant from Br^- to Cl^- or SO_4^{2-}, the mesophase structure of the final PMO materials can be changed from a 2-D hexagonal (*p6mm*) structure to a cubic ($Pm\bar{3}n$) mesostructure, strongly suggesting that the counterions do play an important role in the formation of ethane-bridged PMO materials under basic conditions. Besides the use of a surfactant with different counterions, the addition of inorganic salts is another effective way to introduce different counterions into the synthetic system. In this part of the work, the effect of the counterions is therefore investigated by adding different sodium salts, including $NaNO_3$, NaCl and NaSCN, during the synthesis of ethane-bridged PMOs.

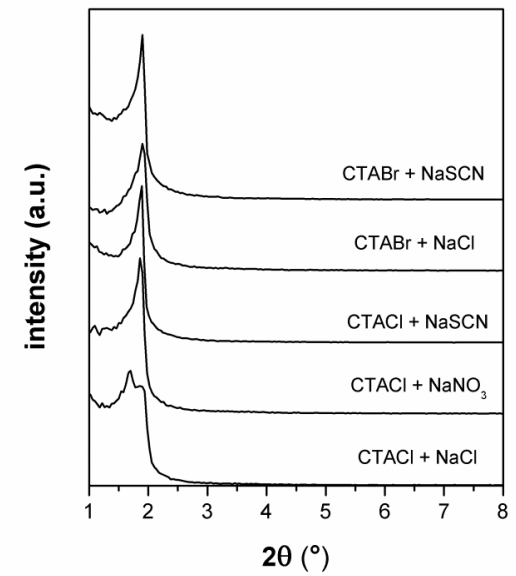

Figure 7. The XRD patterns of as-synthesized ethane-bridged PMOs prepared with the assistance of different sodium salts. All PMOs were prepared with the BTEE silica precursor.

The XRD patterns of the ethane-bridged PMOs prepared with BTEE in the presence of different sodium salts are presented in figure 7. All of the samples exhibit 2-D hexagonal (*p6mm*) mesostructure, except for the PMOs synthesized with CTACl/NaCl giving rise to a cubic ($Pm\bar{3}n$) mesostructure. These results are quite interesting, since in case of PMOs synthesized without the of sodium salts, the use of CTACl can only lead to PMOs with cubic ($Pm\bar{3}n$) mesostructure. However, by adding $NaNO_3$ or NaSCN to the synthesis mixture, the final PMO materials synthesized with CTACl exhibit 2-D hexagonal (*p6mm*) mesostructure, which indicates that the addition of $NaNO_3$ or NaSCN has critically affected the formation of the mesostructure. It should be noted that not all the sodium salts can lead to the mesophase transformation. For example, the addition of NaCl to the CTACl synthetic system gives rise to a PMO with cubic ($Pm\bar{3}n$) mesostructure, which is the same to that of the PMOs synthesized without NaCl. This seems to indicate that the mesophase change is induced by counterion exchange of the template. It is also noteworthy that, depending on the original counterions in the synthetic system, the effect of the sodium salts is different, such as the addition of NaSCN to the CTACl synthetic system resulting in a mesophase transformation of the final PMO from cubic ($Pm\bar{3}n$) phase to 2-D hexagonal (*p6mm*) phase, whereas the addition of NaSCN in the CTABr synthetic system does not cause any change in the mesophase of the final product. However, the morphology is affected by the sodium salts (see supporting information, SEM images).

Effect of silica precursor

In this part of the work, the effect of the silica precursor on the formation of the mesostructure of PMO materials was investigated by using BTME as the organosilica precursor instead of BTEE. Actually, BTEE and BTME are very similar, except for the different silyl groups, namely ethyl and methyl, respectively (scheme 1).

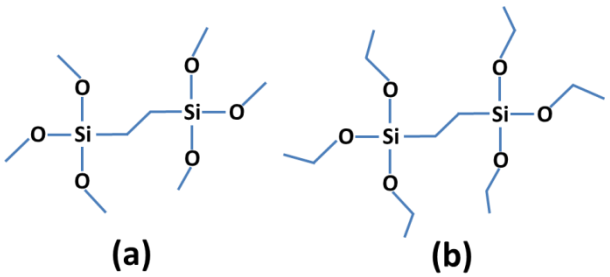

Scheme 1. Chemical structure of the organosilica precursor: (a) BTME and (b) BTEE

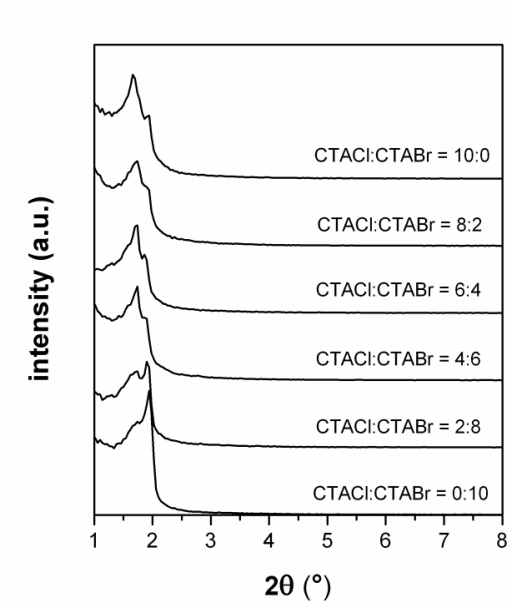

Figure 8 The evolution of the XRD patterns of the as-synthesized ethane-bridged PMOs with BTME, in the presence of a surfactant mixture of CTABr/CTACl with different molar ratios.

Figure 8 shows the XRD patterns of ethane-bridged PMOs synthesized with BTME, in the presence of a surfactant mixture of CTACl/CTABr with different molar ratios. When CTACl : CTABr = 0:10, the XRD pattern of the sample exhibits an intense diffraction peak at 2θ = 2.0° and a weak shoulder peak at 2θ = 1.6°, which is quite similar to the XRD pattern of the PMOs synthesized with CTACl : CTABr = 4:6 when BTEE is used (figure 6a). Indeed, in the case of PMOs synthesized with BTEE, only a 2-D hexagonal (*p6mm*) mesostructure was obtained for CTACl : CTABr = 0:10 or 2:8 (figure 6a). This means that it is difficult to obtain a pure 2-D hexagonal (*p6mm*) mesostructure with the use of BTME. When CTACl : CTABr = 2:8, the PMO synthesized with BTME shows two peaks with similar intensity in the low angle region, suggesting a mixed mesophase (Figure 8). This situation was only observed for CTACl : CTABr = 6:4 when BTEE is used (figure 6a). With further increase of the proportion of CTACl in the surfactant mixture, the PMOs show an XRD pattern consistent with a cubic ($Pm\bar{3}n$) mesostructure. These results indicate that the mesostructure of the final PMO materials can be affected by using different precursors. The use of BTEE favors the formation of 2-D hexagonal (*p6mm*) mesostructure, while cubic ($Pm\bar{3}n$) mesostructure is favored when BTME is used.

Discussion

Effect of counterions from surfactant

We hereby investigated the influence of counterions on the formation of ethane-bridged PMO materials with BTEE as the precursor under basic conditions. To this end, different counterions were introduced into the synthetic system through two different ways. The first way is the direct use of cetyltrimethylammonium surfactant containing different counterions, while the second way involves the addition of different sodium salts to the synthesis mixture.

The advantage of the first method is that the composition of the synthesis mixture, except for the counterions, can be kept always the same, which is indeed an ideal way for investigating the effects of counterions. In the case of the CTABr surfactant, a 2-D hexagonal (*p6mm*) mesostructure was obtained, while a cubic ($Pm\bar{3}n$) mesostructure was obtained in case of CTACl or $CTA(SO_4)_{½}$. Furthermore, with gradually replacing CTABr by CTACl or $CTA(SO_4)_{½}$, a clear mesophase evolution is evidenced by the XRD patterns. The formation of an ordered mesostructure is often difficult to predict due to the complexity of the reaction processes. In our case, all the synthesis conditions are kept identical, except for the counterions, therefore, the change of the mesophase can directly be attributed to the change in counterions.

Actually, changing the counterions is known to have a strong effect on the solution behavior of quaternary ammonium surfactants. For example, the critical micelle concentrations[37], micelle shape[38,39] and phase equilibria[40] can all be influenced by the counterions. Among those, the shape/geometry of the surfactant micelle is essential for the formation of the ordered mesostructure. The packing of the surfactant molecules can be described through the use of the packing parameter, $g = V/a_0l$,[41] where V is the total volume of surfactant hydrophobic chains plus any co-solvent (organic molecules) between the chains, a_0 is the effective hydrophilic headgroup area at the aqueous-micelle surface, and l is the kinetic surfactant chain length. The a_0 parameter is related to both the size and the charge on the surfactant head group and is affected by the electrostatic environment around the surfactant head group. Specific values of g are associated with cubic ($Pm\bar{3}n$) or 3-D hexagonal ($P6_3/mmc$) phase ($g \leq 1/3$), 2-D hexagonal (*p6mm*) phase ($1/3 < g < 1/2$), cubic (*Ia3d*) phase ($1/2 < g < 2/3$), and lamellar (*P2*) phase ($g = 1$). The effects of counterions on the packing of the surfactant molecules can be explained in terms of the different binding strengths on the head groups of the surfactant micelle.[10,42] The counterions will be hydrated in the surfactant solution and the hydrated radii of anions significantly depend on the degree of hydration. For instance, the ionic radius of Br^- is about 0.14 Å larger than the radius of Cl^-. This makes the electrostatic potential of Br^- smaller and the water solvation shell less attached to the anion. Therefore, less strongly hydrated ions (Br^-) have in general smaller ionic radii, and will more closely approach the micelle surface formed by the ammonium head groups. Here, also the rules of the Hofmeister series apply, stating that the binding strength of anions for the cationic surfactant is increased in the following order of $SO_4^{2-} < Cl^- < Br^- < NO_3^- < SCN^-$.[43] Considering that the binding of the anions opposite to the surfactant headgroups would decrease the surfactant repulsion and thus decrease the a_0 value, the value of the packing parameter g will increase in a parallel order: $SO_4^{2-} < Cl^- < Br^- < NO_3^- < SCN^-$.

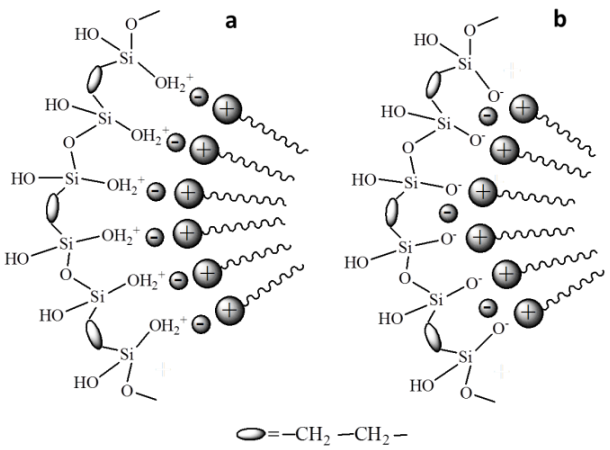

Scheme 2. Proposed synthetic pathway of ethane-bridged PMO materials in the presence of counterions under: (a) acidic media and (b) basic media

The counterions-induced mesophase transformation under acidic condition has been reported by Che et al.[10] and Liu et al.[15] In those cases, the formation of the mesoporous silica follows a $S^+X^-I^+$ model in which the surfactant micelles will always be covered and affected by the counterions during the synthesis (scheme 2a). However, under basic conditions, the mesostructure is constructed through a S^+I^- pathway. It is generally assumed that, in the S^+I^- pathway, the counterions X^- will first cover the surfactant micelle, and then be exchanged by the hydrolyzed silicate species. The counterions X^- act as a block for the adsorption of silicate species to the micellar surface.[16] After being exchanged, the influence of the counterions on the packing of the surfactant becomes less effective. However, our results show that the formation of the mesostructure of ethane-bridged PMOs can be significantly affected by the counterions under basic conditions. A modified synthesis pathway $[S^+mX^-(1\text{-}m)I^-]$ has once been suggested by Bonneviot et al.[32] for the mesoporous templated silicas prepared in basic media. According to this mechanism, the counterions present at the micelle surface cannot be fully exchanged by the silicate species (depending on their binding strength toward the CTA^+ hydrophilic head) and they will remain in the channels of the as-synthesized materials.[36] We have also found

some retained counterions in the as-synthesized ethane-bridged PMO material (supporting information, EDX analysis). Most likely, this mechanism is thus also applicable here and explains how the type of counterion influences the mesostructure of the PMO materials under basic conditions (scheme 2b). It should be noted that, in the previous studies, only pure silica sources, such as fumed silica or TEOS, were used as the silica precursor, and no mesophase changes were observed simply upon varying the counterions in basic conditions. In our case, organosilica precursor BTEE or BTME were used (scheme 1). Due to the organic groups present in the organosilica precursor, the hydrolyzed BTEE or BTME is more hydrophobic compared to the inorganic silica precursor, which will indeed lead to a weaker competition between the silica species and counterions at the interface of the surfactant micelles. Moreover, the organic group within the organosilica precursor may act as a spacer (0.423nm for BTEE/BTME), which allows a fraction of the counterions to remain on the surfactant surface. These factors will probably make the effect of counterions more pronounced when organosilica precursor is used.

Effect of addition of sodium salts

In another series of experiment, the genuine synthesis recipe for ethane-bridged PMOs is modified by adding different sodium salts, including $NaNO_3$, NaCl and NaSCN. It should be noted that this method will introduce additional cations and anions into the synthesis mixture. We have found that the addition of $NaNO_3$ or NaSCN to the CTACl synthesis system can lead to a mesophase transformation of the final product from cubic ($Pm\bar{3}n$) phase to 2-D hexagonal (*p6mm*) phase. Considering that the higher counterion concentrations favor the formation of larger g parameter mesophases,[11,44] it is not certain whether the mesophase transformation is due to the introduction of different counterions or the increase of the counterions concentration. However, the addition of NaCl to the CTACl synthesis system and the addition of NaCl or NaSCN in the CTABr synthesis system does not lead to any mesophase transformation, which suggests that the mesophase transformation in our case is not profoundly affected by the concentration of counterions. Indeed, the mesophase transformation caused by the addition of sodium salts can be explained by the competition between the counterions coming from the surfactant and the counterions coming from the salts. According to the Hofmeister series, the binding strength of counterions to the surfactant is increased in the following order of $SO_4^{2-} < Cl^- < Br^- < NO_3^- < SCN^-$.[42] When CTACl is used, the addition of counterions with larger binding strength, such as NO_3^- or SCN^-, can replace the Cl^- on the surface of the surfactant micelle, leading to a higher value of g parameter, and thus inducing a mesophase change from cubic ($Pm\bar{3}n$)→ 2-D hexagonal (*p6mm*). When CTABr is used, the Br^- on the surface of the micelle can never be replaced by Cl^- that has a weaker binding strength. In the case of NaSCN, the larger binding strength of SCN^- than Br^- will lead to a replacement of Br^-, but the g parameter will still be in the range of $1/3 < g < 1/2$. Therefore, no mesophase change can be observed.

Effect of silica precursor

BTEE and BTME are two of the most commonly used organosilica precursors for PMO materials. Because of their structural similarity, they are often considered as interchangeable. However, our results have indicated that the structure of the final ethane-bridged PMOs can be strongly affected by using a different silica precursor. The use of BTEE favors the formation of 2-D hexagonal (*p6mm*) structure, while BTME favors the cubic ($Pm\bar{3}n$) structure.

In fact, due to the different silyl groups, hydrolysis of BTEE is slower than that of BTME owing to steric hindrance at the larger ethoxide.[45] Our previous *in-situ* spin-probe EPR studies on the formation mechanism of ethane-bridged PMOs have revealed that the reaction rate when BTEE is used is slower than that when BTME is used.[46] Because BTEE is more hydrophobic than BTME, and its hydrolysis rate is slower than that of BTME, the unhydrolyzed BTEE may more readily penetrate into the core of the surfactant micelles. This will indeed increases the V, and thus lead to a larger g value. This may be the reason why BTEE favors the formation of larger g-value mesophases. Moreover, besides the hydrolyzed silicate species, the hydrolysis products for BTEE and BTME are ethanol and methanol, respectively. Since methanol is more hydrophilic, it is situated in the outer boundaries of the surfactant micelles, leading to an enlargement of the effective headgroup area (a_0), thus decreasing the g value.[47] As a result, the use of BTEE favors the formation of a mesophase with larger g value, while the use of BTME favors the smaller g-value mesophase.

Conclusions

In summary, we have reported a facile mesophase control of ethane-bridged PMOs under basic conditions. Accordingly, a *p6mm* to $Pm\bar{3}n$ mesophase transformation can be achieved simply by changing the counterions from Br^- to Cl^- or SO_4^{2-}. Moreover, with gradually replacing CTABr by CTACl or $CTA(SO_4)_{½}$, a clear mesophase evolution has been observed. In addition, the mesophase of the final product can also be controlled by adding different sodium salts. Nevertheless, counterions have been proven to play a significant role in determining the mesophase of the final material under basic conditions in the presence of a cationic surfactant. By understanding the role and behavior of the surfactants' counterions on the mesostructure and morphology of the final material, a further insight in the formation mechanism of ethane-bridged PMOs, and of ordered mesoporous materials in general, has been obtained. Furthermore, we have shown that the hydrolysis and condensation rate of the organosilica precursor is also very important for the formation of different types of mesostructures. The use of BTEE favors the formation of 2-D hexagonal (*p6mm*) structure, while BTME favors the cubic ($Pm\bar{3}n$) structure.

Acknowledgements

The Erasmus Mundus CONNEC program is acknowledged for PhD funding of F.L. Furthermore, the authors acknowledge support by the GOA-BOF project 'Optimization of the structure-activity relation in nanoporous materials', funded by the University of Antwerp.

Notes

[a] Laboratory of Adsorption and Catalysis, Department of Chemistry, University of Antwerp, Universiteitsplein 1, B-2610, Wilrijk, Belgium.
[b] BIMEF Laboratory, Department of Physics, University of Antwerp, Universiteitsplein 1, B-2610, Wilrijk, Belgium.
[c] EMAT, Department of Physics, University of Antwerp, Groenenborgerlaan 171, B-2020 Antwerpen, Belgium.
[d] Flemish Institute for Technological Research, VITO, Boerentang 200, B-2400,Mol, Belgiumenborgerlaan

† Electronic Supplementary Information (ESI) available: [HRTEM images of PMO materials synthesized with CTACl and $CTA(SO_4)_{½}$,

acquired along the [001] direction and different diffraction patterns. SEM images of PMO materials synthesized with a surfactant mixture CTABr/CTACl. SEM images of the PMO materials synthesized with the assistance of different sodium salts. EDX analysis of the as-synthesized PMO materials prepared with different surfactant.]. See DOI: 10.1039/b000000x/

References

1 D. Das, J. F. Lee and S. F. Cheng, *J. Catal*., 2004, **223**, 152-160.

2. S. Hudson, J. Cooney and E. Magner, *Angew. Chem. Int. Edit*, 2008, **47**, 8582-8594.
3. A. Corma, *Chem. Rev.*, 1997, **97**, 2373-2419.
4. U. Diaz, D. Brunel and A. Corma, *Chem. Soc. Rev.*, 2013, **42**, 4083-4097.
5. A. Walcarius and L. Mercier, *J. Mater. Chem.*, 2010, **20**, 4478-4511.
6. R. J. Tian, H. Zhang, M. L. Ye, X. G. Jiang, L. H. Hu, X. Li, X. H. Bao and H. F. Zou, *Angew. Chem. Int. Edit*, 2007, **46**, 962-965.
7. I. I. Slowing, B. G. Trewyn, S. Giri and V. S. Y. Lin, *Adv. Funct. Mater*., 2007, **17**, 1225-1236.
8. M. Vallet-Regi, F. Balas and D. Arcos, *Angew. Chem. Int. Edit*, 2007, **46**, 7548-7558.
9. B. J. Melde, B. J. Johnson and P. T. Charles, *Sensors-Basel*, 2008, **8**, 5202-5228.
10. S. N. Che, H. C. Li, S. Lim, Y. Sakamoto, O. Terasaki and T. Tatsumi, *Chem. Mater.*, 2005, **17**, 4103-4113.
11. S. N. Che, S. Y. Lim, M. Kaneda, H. Yoshitake, O. Terasaki and T. Tatsumi, *J. Am. Chem. Soc*., 2002, **124**, 13962-13963.
12. J. M. Kim and G. D. Stucky, *Chem. Commun.*, 2000, 1159-1160.
13. J. W. Tang, C. Z. Yu, X. F. Zhou, X. X. Yan and D. Y. Zhao, *Chem. Commun.*, 2004, 2240-2241.
14. H. P. Lin, C. P. Kao, C. Y. Mou and S. B. Liu, *J. Phys. Chem. B*, 2000, **104**, 7885-7894.
15. M. C. Liu, H. S. Sheu and S. Cheng, *J. Am. Chem. Soc*., 2009, **131**, 3998-4005.
16. H. P. Lin, C. P. Kao and C. Y. Mou, *Micropor. Mesopor. Mat.*, 2001, **48**, 135-141.
17. H. P. Lin, S. F. Cheng and C. Y. Mou, *Micropor. Mater.*, 1997, **10**, 111-121.
18. B. Echchahed, M. Morin, S. Blais, A. R. Badiei, G. Berhault and L. Bonneviot, *Micropor. Mesopor. Mat.*, 2001, **44**, 53-63.
19. S. Inagaki, S. Guan, Y. Fukushima, T. Ohsuna and O. Terasaki, *J. Am. Chem. Soc*., 1999, **121**, 9611-9614.
20. T. Asefa, M. J. MacLachlan, N. Coombs and G. A. Ozin, *Nature*, 1999, **402**, 867-871.
21. B. J. Melde, B. T. Holland, C. F. Blanford and A. Stein, *Chem. Mater*., 1999, **11**, 3302-3308.
22. M. C. Burleigh, M. A. Markowitz, S. Jayasundera, M. S. Spector, C. W. Thomas and B. P. Gaber, *J. Phys. Chem. B*, 2003, **107**, 12628-12634.
23. S. Hamoudi, Y. Yang, I. L. Moudrakovski, S. Lang and A. Sayari, *J. Phys. Chem. B*, 2001, **105**, 9118-9123.
24. Y. C. Liang, M. Hanzlik and R. Anwander, *J. Mater. Chem.*, 2005, **15**, 3919-3928.
25. H. I. Lee, C. Pak, S. H. Yi, J. K. Shon, S. S. Kim, B. G. So, H. Chang, J. E. Yie, Y. U. Kwon and J. M. Kim, *J. Mater. Chem.*, 2005, **15**, 4711-4717.
26. Y. C. Liang, E. S. Erichsen, M. Hanzlik and R. Anwander, *Chem. Mater.*, 2008, **20**, 1451-1458.
27. L. Y. Xia, Y. C. Hu, Y. Q. Wu, M. Q. Zhang and M. Z. Rong, *J. Sol-Gel Sci. Techn*., 2012, **64**, 718-727.
28. M. P. Kapoor and S. Inagaki, *Chem. Mater.*, 2002, **14**, 3509-3514.
29. W. Guo, F. Kleitz, K. Cho and R. Ryoo, *J. Mater. Chem.*, 2010, **20**, 8257-8265.
30. Y. C. Liang, M. Hanzlik and R. Anwander, *J. Mater. Chem.*, 2006, **16**, 1238-1253.
31. A. Sayari, S. Hamoudi, Y. Yang, I. L. Moudrakovski and J. R. Ripmeester, *Chem. Mater.*, 2000, **12**, 3857-3863.
32. A. R. Badiei, S. Cantournet, M. Morin and L. Bonneviot, *Langmuir*, 1998, **14**, 7087-7090.
33. H. Yang, N. Coombs and G. A. Ozin, *Nature*, 1997, **386**, 692-695.
34. S. S. Park, C. H. Lee, J. H. Cheon and D. H. Park, *J. Mater. Chem.*, 2001, **11**, 3397-3403.
35. S. Guan, S. Inagaki, T. Ohsuna and O. Terasaki, *J. Am. Chem. Soc*., 2000, **122**, 5660-5661.
36. Y. Guillemin, J. Ghanbaja, E. Aubert, M. Etienne and A. Walcarius, *Chem. Mater*., 2014, **26**, 1848-1858.
37. A. L. Underwood and E. W. Anacker, *J. Colloid Interf. Sci.*, 1985, **106**, 86-93.
38. T. Imae, R. Kamiya and S. Ikeda, *J. Colloid Interf. Sci.*, 1985, **108**, 215-225.
39. F. Quirion and L. J. Magid, *J. Phys. Chem.-Us*, 1986, **90**, 5435-5441.
40. E. S. Blackmore and G. J. T. Tiddy, *J. Chem. Soc. Farad. T 2*, 1988, **84**, 1115-1127.
41. Q. S. Huo, D. I. Margolese and G. D. Stucky, *Chem. Mater*., 1996, **8**, 1147-1160.
42. E. Leontidis, *Curr. Opin. Colloid Interface Sci*. 2002, **7**, 81-91.
43. D. N. Rubingh and P. M. Holland, *Cationic surfactant: Physical Chemistry, surfactant science series*, 1991, **37**.
44. S. Ozeki and S. Ikeda, *J. Colloid Interf. Sci*., 1982, **87**, 424-435.
45. H. S. Xia, C. H. Zhou, D. S. Tong and C. X. Lin, *J. Porous. Mat*., 2010, **17**, 225-252.
46. L. Feng, M. Mertens, P. Cool and S. Van Doorslaer, *J. Phys. Chem. C*, 2013, **117**, 22723–22731.
47. G. R. Zhu, Q. H. Yang, H. Zhong, D. M. Jiang and C. Li, *J. Phys. Chem. B*, 2007, **111**, 8027-8033.